An integrated approach to highlight biological responses of Pisum sativum root to nano-TiO2 exposure in a biosolid-amended agricultural soil

(Article begins on next page)

1 **An integrated approach to highlight biological responses of *Pisum sativum***

2 **root to nano-TiO₂ exposure in a biosolid-amended agricultural soil.**

3

4 **Giorgetti L.[1*], Spanò C.[2*], Muccifora S.[3], Bellani L.[1,3], Tassi E.[4], Bottega S.[2], Di Gregorio**

5 **S.[2], Siracusa G.[2], Sanità di Toppi L.[2], Ruffini Castiglione M.[2]**

6

7 *Co-first Authors

8 [1] Institute of Agricultural Biology and Biotechnology, UOS Pisa, CNR, Via Moruzzi 1, 56124

9 Pisa, Italy

10 [2] Department of Biology, University of Pisa, Via Ghini 13, 56126 Pisa, Italy

11 [3] Department of Life Sciences, University of Siena, Via A. Moro 2, 53100 Siena, Italy

12 [4] Institute of Ecosystem Studies, National Research Council (ISE-CNR), via Moruzzi 1,

13 56124 Pisa, Italy

14

15 Corresponding author:

16 Monica Ruffini Castiglione, Department of Biology, University of Pisa, Via Ghini 13, 56126

17 Pisa, Italy. E-mail: monica.ruffini.castiglione@unipi.it

18 Tel. +390502211317

19

20

21

22

23

24

25

26 **Abstract**

27 This study focused on crop plant response to a simultaneous exposure to biosolid and TiO_2 at

28 micro- and nano-scale, being biosolid one of the major sink of TiO_2 nanoparticles released

29 into the soil environment. We settled an experimental design as much as possible realistic, at

30 microcosm scale, using the crop *Pisum sativum.* This experimental design supported the

31 hypotheses that the presence of biosolid in the farming soil might influence plant growth and

32 metabolism and that, after TiO_2 spiking, the different dimension and crystal forms of TiO_2

33 might be otherwise bioavailable and differently interacting with the plant system. To test

34 these hypotheses, we have considered different aspects of the response elicited by TiO_2 and

35 biosolid at cellular and organism level, focusing on the root system, with an integrative

36 approach. In our experimental conditions, the presence of biosolid disturbed plant growth of

37 *P. sativum*, causing cellular damages at root level, probably through mechanisms not only

38 oxidative stress-dependent but also involving altered signalling processes. These disturbances

39 could depend on non-humified compounds and/or on the presence of toxic elements and of

40 nanoparticles in the biosolid-amended soil. The addition of TiO_2 particles in the sludge-

41 amended soil, further altered plant growth and induced oxidative and ultrastructural damages.

42 Although non typical dose-effect response was detected, the most responsiveness treatments

43 were found for the anatase crystal form, alone or mixed with rutile. Based on ultrastructural

44 observations, we could hypothesise that the toxicity level of TiO_2 nanoparticles may depend

45 on the cell ability to isolate nanoparticles in subcellular compartments, avoiding their

46 interaction with organelles and/or metabolic processes.

47 The results of the present work suggest reflections on the promising practice of soil

48 amendments and on the use of nanomaterials and their safety for food plants and living

49 organisms.

50

53

54

55 **1. Introduction**

56

57 Contaminants of emerging concern are increasingly gaining ground in all the ecosystems, due

58 to the unintentional or intentional release into the environment of new molecules/compounds

59 or to a new employment and disposal of complex and potentially polluted matrices (Halden

60 2015). In this context, the reuse of sludge from wastewater treatment plants (WWTP) in

61 farming soils is recognized as a cost-effective practice to dispose of a byproduct that can be

62 applied to the soil-plant system as a fertilizer, rich in organic matter and nutrients (Lu et al.

63 2012; EPA 1994). Regulations governing the reuse of biosolid (Bs) in farming applications

64 take several broad forms in different countries, but basically they follow a code of good

65 practice, which foresees specific treatments and maturation aimed to guarantee defined

66 chemical, physical and microbiological standards (EEC 1986; EPA 1993).

67 On the other hand, due to the uncertainty of its content not thoroughly tested for safety, Bs

68 can result a possible sink of organic and inorganic unknown priority pollutants as well as of

69 not commonly monitored chemicals, such as nanoparticles (NPs) (Brar et al. 2010; Yang et al.

70 2014).

71 The nanotechnology revolution and its challenges has been going on for some time,

72 accompanied however by a series of ethical/safety implications related to the release into the

73 environment of new nano-chemical compounds whose effects on ecosystems and living

74 organisms are not yet fully clear and unambiguously interpretable (Maurer-Jones et al. 2013).

75 Besides, NPs behavior is poorly estimated in the different environmental matrices, especially

76 in agricultural soils. In such complex matrices, the bioavailability of the different NPs often is

77 not predictable, due to their tendency to aggregate, to adsorb/precipitate on solid phase, as

78 well as to be coated by organic molecules (Tourinho et al. 2012; Pachapur et al. 2016). In

79 addition, the overall picture of their possible interactions with crop plants and with food

80 chains are not at all clear (Ruffini Castiglione and Cremonini 2009; Remedios et al. 2012;

81 Rico et al. 2011; Tassi et al. 2017). Given that we can not afford to miss the opportunity of

82 exploiting nanotechnologies, it is priority and urgent to dispel these uncertainties, that

83 nowadays remain, about the possible harmful effects of these nanomaterials, otherwise

84 transferred in farming soils, on crop plants and food chains.

85 TiO$_2$ NPs are among the top five nanomaterials widely used for various applications

86 (Chuankrerkkul and Sangsuk 2008), ranging from food and personal care products (Weir et

87 al. 2012) to specific medical devices coating (Villatte et al. 2015) and drug delivery systems

88 (Bakhshizadeh et al. 2017), from coating pigments production (El-Sherbiny et al. 2014) to

89 their employment in certain farming sectors and in environmental cleanup technologies

90 (Bhawana and Fulekar 2012; Liu 2011). A broad sector of the current body of literature on the

91 environmental impact of NPs is focused on this class of nanomaterials: in recent years, the

92 number of studies on their effects on higher plants is increasing, as well as the different

93 experimental approaches and endpoints considered to evaluate NPs uptake, translocation,

94 accumulation in plant tissues/organs and potential toxicity (Larue et al. 2012; Song et al.

95 2013; Ruffini Castiglione et al. 2014, Ruffini Castiglione et al. 2016; Amini et al. 2017). The

96 researchers' guidance on these issues is also connected to the general awareness and concern

97 that the most used NPs, including TiO$_2$, may easily and in a short time reach significant

98 environmental concentrations and enter in the food chains through crop plants, thus affecting

99 the whole living organisms (Rico et al. 2011).

100 Most of the works published so far on TiO$_2$ NPs effects on plants of agronomic interest report

101   data obtained in hydroponics, water suspensions or under any other experimental conditions

102   to monitor the short-term effects, testing high concentrations of TiO_2 (Maurer-Jones et al.

103   2013; Cox et al. 2016), often not realistic, even in the case of accidental pollution (Sun et al.

104   2014). In this context, there are few studies involving the use of agricultural soils as growth

105   substrates for plants along with the application of treatments (Du et al. 2011; Burke et al.

106   2014; Gogos et al. 2016).

107   In this report, we settled an experimental design as much as possible realistic, at microcosm

108   scale, using a biosolid-amended agricultural soil as growth matrix for the crop *Pisum sativum.*

109   We aimed to investigate the effects of TiO_2 in the form of bulk material and in three different

110   nanoparticulate formulations: crystals of anatase, rutile, and a mix of both, all applied at two

111   different concentrations in the range established simulating an environmental contamination,

112   and under long term exposure. This experimental design supports the hypotheses that the

113   presence of Bs in itself may influence plant growth and metabolism and that, after TiO_2

114   spiking, the different dimension and crystal forms of titanium dioxide might be otherwise

115   bioavailable and differently interacting with the plant system. To test our hypotheses, we have

116   chosen to take into account different aspects of the response elicited by TiO_2 and Bs in

117   tissues/organs, at cellular and organism level, focusing on the root system, with an integrative

118   approach.

119

120

121

122   **2. Materials and Methods**

123

124   *2.1 Growth substrates*

125   The farming soil (C1) was collected at CiRAA - Agri-Environmental Research Center 'Enrico

126   Avanzi' from University of Pisa, Italy. The soil was air-dried, sieved (0-2 mm) and

127   homogenized before its analysis and use as growth substrate. C1 soil was characterized by a

128   sandy texture (93.3% of sand, 4.6% of silt and 2.1% of clay) with a pH near the neutrality

129   (7.7), low organic matter content (OM, 1.1%), medium value of cation exchange capacity

130   (CEC, 15.5 cmol$^{(+)}$ kg^{-1}) and electrical conductivity (EC) of 0.80 mS cm^{-1}.

131   Bs was obtained from a small WWTP in Pisa (Italy) as a dewatered sludge qualified for its

132   use in an agricultural soil. Bs was further characterized by having a solid residue (at 105°C)

133   of 18%, pH of 6.9, high OM (57.3%), EC of 11.5 mS cm^{-1} and total concentration of Ti of

134   699 ± 105 mg kg-1 (dw basis). Titanium background found in Bs is in line with that from

135   other studies and model predictions (Josko and Oleszczuk, 2013; Kim et al. 2012; Sun et al.

136   2014). Heavy metals (As, Cd, Cr, Hg, Ni and Pb), PAH (polycyclic aromatic hydrocarbons)

137   and *Salmonella spp.* content were all below the limit of law reference for its use in farm soils

138   (Italian Legislative Decree 99/92 and Commission Regulation (EU) n° 1357/2014).

139   Commercial powder of TiO_2 was bought from US Research Nanomaterials Inc. (Houston,

140   USA) as anatase or rutile NPs (nominal size of 30 nm) and from Sigma-Aldrich (Saint Louis,

141   USA) as bulk particles (>100 nm), all having at least 99.9% of purity (producers'

142   information).

143   Different growth substrates were prepared and designed as follows: 1) C1 = farming soil; 2)

144   C2 = farming soil enriched with 3% of Bs (dry weigh basis); 3) A = C2 + nano anatase; 4) R

145   = C2 + nano rutile; 5) Mix = C2 + anatase + rutile (1:1 ratio); 6) B = C2 + bulk TiO_2. For the

146   preparation of growth substrates 3) – 6) TiO_2 in nano and bulk sizes were suspended, at

147   appropriate concentrations, in milli-Q water using a sonicator (Sonifier 250, Branson) for 30

148   min at 80 W to simulate, through the Bs amendment, low and high dose TiO_2 loading in the

149   soil (80 and 800 mg TiO_2 kg^{-1} of soil, respectively). TiO_2 concentrations were chosen as

150   representative amounts of best- and worst-case scenarios of nanoparticles load through

151 biosolids in farm soils (Sun et al. 2014). TiO_2 suspensions and Bs were mixed mechanically

152 for 24 hs and left in open-air for 30 d with occasional mixing to permit the possible nano or

153 bulk particles transformations in the biosolid and the evaporation of excess water. The

154 resulting substrate material (Bs+TiO_2) was blended with the agricultural soil to obtain the

155 growth substrates A, R, Mix and B with nominal TiO_2 concentrations of 80 and 800 mg kg^{-1}

156 soil (dry-weight basis). C2 control soil was subjected to the same procedure without the TiO_2

157 addition. In comparison with C1, the C2 displayed increase of some agronomical parameters:

158 OM (3.1 times), CEC (1.5 times), EC (2.6 times), N_{tot} (5.7 times), P_{tot} (14.7 times), Ca (1.4

159 times), Mg (2.3 times), Cu (7.4 times) and Zn (4.1 times). Moreover, the pH was slightly

160 reduced to neutrality (7.01) and the texture remained unaltered.

161

162 *2.2 Plant material and growth conditions*

163 *Pisum sativum* L. seeds, homogeneously selected, were soaked in water over night and then

164 transferred to pots containing 500g of the growing substrates described above. Four pots per

165 treatment sowed with ten seeds per treatment were randomly disposed in a growth-room

166 under controlled conditions (16/8 h light/dark photoperiod, 22/16 °C) re-adjusting daily the

167 moisture of growth substrate with tap water. After 28d, plants were collected and root length

168 was measured. The roots were isolated, carefully washed with tap water and rinsed with

169 deionized water. Possible adhered soil particles in the roots were further eliminated by

170 sonication in deionized water using a pulse mode and an output power of 15W for about

171 5min. Fresh root samples were used for histochemical analysis, fixed for structural and

172 ultrastructural observations or stored at -80°C until use for biochemical determinations.

173

174 *2.3 Ti analysis in soils and plants*

175 The fraction of Ti available in soils, determined through a single extraction with

176   diethylenetriaminepentaacetic acid (DTPA), represents an operational method for the

177   determination of the fraction potentially accessible for plants uptake (Rauret 1998).

178   This bioavailable portion of Ti in the different growth substrates was determined using 0.01M

179   DTPA, following the procedure in Methods of Soil Analysis (SSSA 1996). Soil extracts were

180   volume reduced until almost dryness before Ti analysis. A portion of well-washed roots was

181   oven-dried and grounded to fine powder. Both, soil extracts and roots samples, were

182   mineralized in an open-block-digestor in two steps: after digestion with $HNO_3 + H_2O_2$, the

183   volume of liquid was reduced to almost dryness and the residue was re-digested with H_2SO_4

184   (Fang et al. 2009). Ti in the digested samples was determined by Inductively Coupled Plasma

185   Optical Emission Spectrometry (ICP-OES, Varian Liberty Axial). Control and assurance of Ti

186   analysis by ICP-OES were performed testing the two standard solutions (0.5 and 2 mg L-1)

187   every 5 samples. The same TiO_2 NPs employed in the experiments (Houston, USA) have

188   been used as a reference material for digestion method and Ti analysis, where the recovery

189   level (as TiO_2) ranged from 91% to 103% with a relative standard deviation of the mean of

190   2.95.

191

192   *2.4 Histochemical detection of oxidative stress on root system*

193   Five roots of comparable size and length, randomly selected from control and treated plants,

194   were excised and sectioned with hand microtome in correspondence to the initial root hair

195   area. Cross sections were immediately processed with fluorescent probes specific for

196   hydrogen peroxide and lipid peroxidation. Fluorescent Amplex UltraRed Reagent (Life

197   Technologies, USA) was applied for *in situ* detection of H_2O_2 following manufacturing

198   instructions and protocol reported in Ruffini Castiglione et al. (2016). After staining, slices

199   were mounted in glycerol and observed with fluorescence microscope (568ex/681em nm).

200   BODIPY 581/591 C11 was used as free radical sensor to visualize lipid peroxidation levels as

201   a change of the fluorescence emission peak from red to green. The slices were incubated and

202   stained following a previous protocol (Ruffini Castiglione et al. 2016). Microscope evaluation

203   was performed acquiring simultaneously the green (485ex/510em nm) and the red

204   fluorescence (581ex/ 591em nm) signals and merging the two images (Kovácik et al. 2014).

205   Fluorescence microscope analysis was carried out with a Leica DMLB, equipped with

206   appropriate set of excitation/emission filters and with a Leica DC300 ccd camera.

207

208   *2.5 Extraction and determination of hydrogen peroxide and thiobarbituric acid reactive*

209   *substances (TBARS)*

210   Hydrogen peroxide content of roots was determined according to Jana and Choudhuri

211   (1982). Briefly, roots were ground in a mortar and homogenised with phosphate buffer 50

212   mM pH 6.5. The homogenate was centrifuged at 6,000 g for 25 min. To determine the

213   H_2O_2 content, 3 ml of extracted solution were mixed with 1 ml of 0.1% titanium chloride in

214   20% (v/v) H_2SO_4, then the mixture was centrifuged at 6,000 g for 15 min and the

215   supernatant absorbance was read (410 nm). The amount of H_2O_2 in the extracts was

216   calculated from a standard curve and expressed as μmol g^{-1}FW.

217   Lipid peroxidation in roots was measured by detecting the amount of TBARS determined

218   by the thiobarbituric acid (TBA) reaction, according to Hartley-Whitaker et al. (2001) with

219   minor modifications as in Ruffini Castiglione et al. (2016). Briefly, roots were mixed with

220   TBA reagent (10% w/v trichloroacetic acid + 0.25% w/v thiobarbituric acid), heated (95°C

221   for 30 min), cooled for 15 min and centrifuged at 2,000 g for 15 min. The level of TBARS

222   was measured as specific absorbance at 532 nm by subtracting the non-specific absorbance

223   at 600 nm and calculated using an extinction coefficient of 155 mM^{-1} cm^{-1}. TBA-reactive

224   materials were expressed in nmol g^{-1} FW.

225

226 *2.6 Transmission electron microscopy (TEM)*

227 In order to evaluate morphology and size of nanoparticles, suspensions in milli-Q water were

228 prepared at 80 mg kg^{-1} and a drop (10 μL) was placed on TEM grids covered with formvar

229 and allowed to settle. The grids were stained with uranyl acetate, washed and left to dry. For

230 root observations, small root cubes (2x2 mm) of control and of each treatment were pre-fixed

231 in Karnovsky solution (Karnovsky 1965), post-fixed in osmium tetroxide, dehydrated and

232 embedded in Epon 812-Araldite A/M mixture. Thin sections were stained with uranyl acetate

233 and lead citrate.

234 Isolated NPs and root sections were observed under a FEI Technai electron microscope at

235 100kv.

236

237 *2.7 Statistical analysis*

238 Statistical analysis was performed using the Statistica package (StatSoft) version 6.0. All the

239 data were the mean of at least three replicates from three independent experiments. The

240 differences among means of the two control samples (C1 and C2) were compared using T

241 student test. Effects of treatments (form: anatase and rutile; size: nano and bulk), of the two

242 concentrations and their interaction were analyzed using two-way ANOVA. The differences

243 among means were compared with a *post-hoc* analysis of variance using Tukey test (Tukey

244 Honestly Significant Difference) at $p < 0.05$.

245

246 **3. Results**

247 *3.1 Titanium in soils and roots*

248 Titanium analysis in the soil extracts and in the biomass of roots were represented in Fig 1.

249 The concentration of Ti bioavailable in the soils ranged from 290 to 625 μg kg^{-1}. The

250 presence of biosolid did not affect the available fraction of Ti in the soil since no significant

251 differences were observed between C1 and C2. Ti spiking (through the Bs soil amendment)

252 induced significant differences in Ti content in the soil in function of different treatments

253 (F=13.91, P<0.001) and concentrations (F=27.97, P<0.001), particularly evident for A800

254 showing a significant increase (about 70%) in respect to C2 (Fig. 1). Statistical significant

255 interaction between treatments and concentration (F=11.25, P<0.001) was observed.

256 Titanium accumulation in the roots (Fig. 1) was similar in the C1, C2 and in the roots from

257 low dose in all the treatments, with significantly higher accumulation than C2 found in all the

258 high dose treatments (F=74.935, P<0.0001), R800 and B800 displaying differences with

259 statistical significance.

260

261 *3.2 Root growth and oxidative stress*

262 After 28 days, C2 plants displayed reduced root length in comparison to C1 plants (Table 1a).

263 Moreover, our data indicated a further significant root growth inhibition under TiO_2

264 treatments (F=13.154, P<0.0001), the lowest value characterising A80, followed by B800 and

265 B80 (Table 1b), with no significant effect for concentration (F=2.475, P=0.119) and

266 interaction between the two factors (F=2.348 P=0.0589).

267 In Table 1a not significant differences in H_2O_2 content between the roots of the two controls

268 were observed. In comparison with C2, all the treated materials had higher concentration of

269 this signalling molecule (Table 1b), in function of treatments (F=9.967, P<0.0001) and

270 concentration (F=16.468, P<0.0001), the highest content being reached in A80, followed by

271 Mix80, B800 and R800 (in decreasing order). The lowest content of H_2O_2 was observed in

272 Mix800. A significant interaction was observed between the two factors (F=24.078,

273 P<0.0001).

274 C2 and C1 had comparable concentrations of TBARS, indicative of lipid peroxidation and of

275 membrane damage (Table 1a). NPs treatments significantly influenced TBARS content

276   (F=12.257, P<0.0001), Mix800 showing the highest concentration of TBARS and the other

277   treatments having lower values than C2 except for A80 and Mix 80. No significant effect was

278   distinguished for concentrations (F=0.3103, P=0.582), while a significant interaction was

279   observed between the two factors (F=4.752, P<0.0001) (Table 1b).

280

281   *3.3 Histochemical analyses*

282   Specific fluorescent probes were exploited for *in situ* detection of H_2O_2 and lipid peroxidation

283   to achieve qualitative signals related to the oxidative stress.

284   After Amplex UltraRed probe staining (Fig. 2), root cross sections of C1 and C2 samples

285   showed both a faint signal in the cortical cylinder, except for the endodermis, that resulted

286   distinctly stained in the portions facing towards phloem arcs in C2 sample. Central cylinder

287   was more reactive in C2 samples both in the phloematic and mostly in the xylematic arcs.

288   R80 displayed similarity with the C1 staining pattern with reference to the central cylinder,

289   even if in the cortical cylinder the red signal was restricted at the area surrounding the stele.

290   At the high TiO_2 dose treatments, rutile (R800) induced high levels of H_2O_2 in the central

291   cylinder, especially in phloem tissues, and in the inner part of cortical cylinder.

292   A80 and A800 root cross sections displayed a staining pattern strongly involving phloem

293   tissues, and, to a lesser extent, xylem vessels and cortical area, with a high overall staining

294   intensity in A80 samples.

295   Mix800 was the less reactive sample to Amplex UltraRed staining, with a faint signal

296   engaging basically the vascular tissue system, accompanied by uneven weaker signal on the

297   cortical cylinder. Mix80, on the contrary, showed a greater signal intensity in all root

298   compartments extended to the cortical cylinder, including the endodermic layer, facing

299   towards the phloematic arches, and vascular tissues.

300 The roots belonging to plants treated with B80 and B800 mainly showed positivity to the

301 H_2O_2 fluorescent probe in the inner part of cortical cylinder and a peculiar strong staining

302 signal in the rizodermis. Vascular tissue system was as well responsive, especially the phloem

303 tissues of B800.

304 BODIPY 581/591 C11 fluorescent probe is able to identify lipid peroxidation as a change of

305 the fluorescence emission peak from red to green. C1 and C2 samples showed a faint green

306 signal restricted to the cortical region closest to the root central cylinder (Fig. 3). The green

307 fluorescence was observed in the same root compartment in the samples A80, Mix800 and

308 Mix80. In this latter, the green signal also spread the central cylinder. A800 and R800

309 displayed a preferential green staining to the central cylinder, involving also vascular system

310 as well as the inner part of the cortex. R80 sample was the most similar to C2. B80 and B800

311 reacted to the fluorescent probe with a different pattern of staining, that was mainly

312 recordable in the outer and inner portion of the cortical cylinder (Fig. 3).

313

314 *3.4 TEM observations*

315 The TiO$_2$ anatase NPs (Fig. 4a) were extremely heterogeneous in shape, generally they

316 appeared prismatic or cylindrical in shape; their size was variable from 20 to 80 nm. The

317 rutile NPs were prismatic with cusp and size from 30 to 100 nm (Fig. 4b). Both anatase and

318 rutile NPs appeared highly aggregate.

319 Sections of C1 roots showed cells with large vacuoles with scanty materials evident (Fig. 4c).

320 The thin layer of cytoplasm was rich in endoplasmic reticulum cisternae, dictyosomes,

321 mitochondria and plastids (Fig. 4c).

322 The cells of samples grown in C2 showed ultrastructure similar to that of cells of C1. Often

323 the chromatin was condensed and mitochondria had swollen cristae (Fig. 4d). Some NPs of

324 size 30-50 nm were observed adherent to cellular walls mainly in parenchyma (cortex) cells

325 near to central cylinder (Fig. 4e). In the parenchyma (cortex) cells near to rizoderma

326 aggregates of dense particles (up to 100 nm) were evident (Fig. 4f).

327 In R treated roots cells were often empty or showed more or less evident plasmalemma-wall

328 detachment as in plasmolysis. In the vacuoles of these cells disperse materials and dense NPs

329 of about 20-30 nm were present (Fig. 5a). Furthermore, in these vacuoles wide zones of

330 degenerated cytoplasm were present, often surrounded by a double membrane, with not

331 recognizable organelles and more or less large vesicles containing dense round profiled NPs

332 of about 30 nm in size (Fig. 5b).

333 In A treated roots cells appeared empty or in evident plasmolysis state, as R treated roots cells.

334 Not recognizable organelles or mitochondria with swollen *cristae* and with large crystals (Fig.

335 5c) and nuclei with highly condensed chromatin were evident (Fig. 5d). NPs single or

336 aggregated of about 20-40 nm in size were present in the cytoplasm (Fig. 5e). In vacuoles

337 scattered material with NPs of about 30 nm in size, and vesicles surrounded by a double

338 membrane containing NPs of the same dimension were present (Fig. 5f). In the parenchyma

339 (cortex) cells near to rizoderma, NPs of 20-50 nm in size were observed in organelles,

340 probably mitochondria (Fig. 6a) in portions of cytoplasm (Fig. 6b), adherent or crossing cell

341 wall (Fig. 6c) and in intercellular spaces (Fig. 6d).

342 The cell ultrastructure of Mix treated roots were similar to that described for both A and R

343 treated root cells, namely: evident plasmolysis and disrupted cytoplasm and organelles. The

344 NPs were dispersed in vacuoles, in vesicles surrounded by a double membrane and in

345 cytoplasm (data not shown).

346 The cells of B treated roots were mostly empty, the only organelles detected were the nuclei,

347 often in number of two *per* cell (Fig. 6e). Large nanoparticles and particles of different

348 polyhedral form, isolated or aggregated, were present in parenchyma (cortex) cells near to

349 rizoderma (Fig. 6f).

14

350 No differences in ultrastructure and NPs content were noted in all the samples treated with the

351 two different concentrations.

352

353

354 **4. Discussion**

355 Our study focused on crop plant response to a simultaneous exposure to biosolid and TiO_2 at

356 micro- and nano-scale, whose co-presence may really occur in farm soils (Chen et al. 2017).

357 Generally, the soil treatments with Bs and Bs+TiO_2 did not significantly modify the Ti

358 available fraction in soils, indicating, in this respect, a non-substantial influence of the

359 amendment/spiking on the growth matrix. Exception was found for A800, suggesting a lower

360 entrapment or precipitation of anatase NPs as homo/hetero-aggregates with soil components

361 and producing a significant increase in the Ti bioavailable. Indeed, in soils, the association of

362 multiple factors, including their inorganic and organic constituents and the crystallographic

363 features of NPs, has been reported as the drivers for the TiO_2 behaviour and availability

364 (Laxma Reddy et al. 2016; Tassi et al. 2012).

365 Even if Ti is not an essential nutrient element, in our experimental conditions *P. sativum* roots

366 were able to accrue Ti at concentration levels in some respects even higher than specific

367 essential mineral elements (Lyu et al. 2017) and this was generally recorded regardless of the

368 presence of Bs or nano (and bulk) TiO_2 particles in soil. Only at the high dose treatments *P.*

369 *sativum* roots increased at a certain extent their Ti content, the statistical significance being

370 limited to R800 and B800.

371 The effect of TiO_2 treatments on the root growth of *P. sativum* differed mainly depending on

372 the crystalline form. In accordance with Pittol et al. (2017), TiO_2 NPs treatments induced a

373 reduction in the root growth and the inhibiting action of the micro-scale form (bulk) was

374 confirmed (Ruffini Castiglione et al. 2016). At the low dose treatments, anatase was more

375 toxic than rutile for growth, confirming the higher toxicity of this crystal form in these

376 conditions (Siddiqi and Husen 2017). On the other hand, it must be emphasized that the high

377 dose treatments induced a less negative effect on root elongation, however, significant only

378 for anatase. The mitigation of anatase phytotoxic effect at high concentration has been

379 reported in literature and could be due to the suggested antimicrobial properties of this

380 crystalline form, which increases plant stress resistance (Zheng et al. 2005; Siddiqi and Husen

381 2017). The total Ti content in the root did not differ respect to the controls, despite the

382 increase in the availability of Ti recorded in A800. These results suggest that a multifaceted

383 mechanism of TiO_2 action is present in a such complex matrix, as is the Bs-amended soil, and

384 that it is difficult to foresee/hypothesize the effects which can result in opposite and

385 compensatory responses of the plant.

386 A correlation between the inhibition of growth and the generation of reactive oxygen species

387 (ROS), resulting in oxidative stress, has often been suggested (Prakash and Chung 2016). This

388 was only partially confirmed in our results, where the highest H_2O_2 concentration was

389 associated with the highest inhibition of root growth just in some samples. In fact a non-

390 typical dose-effect relationship for oxidative stress markers seemed to characterize the plant

391 response in our experimentation, probably not weird for NPs spiked into a complex growth

392 matrix (Bell and Ives 2014; Simonin et al. 2016). In addition, and in contrast with Ruffini

393 Castiglione et al. (2016), the highest contents of this ROS were not associated with the

394 highest membrane damages (assessed as TBARS).

395 To complement structure-function analysis, within a project based on an integrated approach,

396 interesting information may derive from the histochemical detection of oxidative stress and

397 the electron microscopy approach, that, though providing semiquantitative/qualitative data,

398 can highlight any differences in the pattern and distribution of oxidative markers, as well as in

399 the cell ultrastructure.

400   Histochemical data, in some respects remind biochemical quantitative results, basically with

401   no specific differences between C1 and C2 samples for both the probes; notwithstanding this,

402   H_2O_2 staining pattern seems more defined for C2 sample, indicating an H_2O_2 production not

403   limited to a normal aerobic metabolism or physiological signalling processes.

404   This behaviour in C2, together with the significant inhibition of root growth, could be

405   ascribed to elements as Cu and Zn that, in accordance with literature (Wen et al. 2002),

406   increased compared to the original soil, of 7.4 times and 4.1 times respectively. These

407   elements notoriously affect the root elongation (Muccifora 2008; Li et al. 2012) and H_2O_2

408   content (Thounaujam et al. 2012; Li et al. 2013). Equally, non-humified compounds resulting

409   from an incomplete biodegradation of organic matter from Bs, such as phenols and ammonia,

410   could cause toxicity in plants (Britto and Kronzucker 2002; Zubillaga and Lavado 2006).

411   Moreover, in C2, NPs of 30-50 nm and large dense particles recorded by TEM analysis and

412   never relieved in C1, could come from the biosolid and be responsible of feeble ultrastructural

413   and histochemical differences between the two controls.

414   The addition of TiO_2 NPs to C2 growth substrates induced distinct histochemical staining

415   patterns allied to H_2O_2 and lipid peroxidation, relating to specific root compartments and

416   depending on the different treatments. These results, in addition with biochemical quantitative

417   data, provide further useful clues, that allow to reveal differences not appreciable with a mere

418   quantitative approach and demonstrating that plant root tissues are differently affected

419   depending on the different TiO_2 crystalline form. For the plants treated with nanoTiO$_2$ the

420   location of H_2O_2 signal in the cortical cylinder in general corresponds to the lipid peroxidation

421   pattern by the BODIPY probe. The apparent contradiction with biochemical results, that

422   seemed to exclude a clear correlation between hydrogen peroxide concentration and TBARS

423   content, further highlights the importance of a multiple approach to better characterize the

424   actual condition of plant material. Interestingly, H_2O_2 positive signal was recurrently

425   observed in correspondence of the vascular tissues. Xylem parenchyma cells supply the H_2O_2

426   required for lignification in differentiating xylem vessels (Barceló 2005). H_2O_2 production

427   and cell-wall lignification increase as oxidative stress response (Kim and Barbara 2008), in

428   our case particularly evident for C2, A80, Mix80 treatments. The presence of H_2O_2 in phloem

429   tissues may be a possible occurrence, being previously described following biotic stress

430   (Walz et al 2002; Musetti et al. 2005) as well as elicited by TiO_2 nanoparticles (Ruffini

431   Castiglione et al. 2016). This occurring may be the result of a systemic stress responses

432   (Wendehenne et al. 2014) in which phloem is involved, changing its transport capacity and

433   the type of molecules/gene products moved (Petrov and Van Breusegem 2012; Liang et al.

434   2014).

435   Although the ultrastructural pattern did not highlight differences depending on the

436   concentration of TiO_2 particles, TEM analysis turned out to be a precocious marker of further

437   evident damages, allowing a fine-tune monitoring of the cell/tissue response to TiO_2 NPs.

438   The electron microscope observation corroborated the presence of both anatase and rutile

439   NPs, confirming their ability to overcross plant root barriers and penetrate the different

440   root/cell compartments (Wang et al. 2016). The most damaged root areas generally

441   corresponded to those identified by histochemical analysis and cell and chromatin

442   ultrastructure appeared more harmed in A than in R treated samples, confirming, also with

443   this approach, the highest toxicity of anatase crystals in plants (Siddiqi and Husen 2017) or

444   minor ability of their detoxification.

445   Indeed, based on our results, we could hypothesise that the toxicity of TiO_2 NPs may depend

446   on the cell ability to isolate them in subcellular compartments, avoiding their interaction with

447   organelles and/or metabolic processes. Though a fraction of anatase NPs was confined in

448   vesicles and in autophagosome-like structures, as previously shown in response to NPs stress

449   (Ruffini Castiglione et al. 2016), most of them was observed free in the cytoplasm and in

450 degenerating organelles as if the ability of the detoxification system was exceeded. On the

451 contrary, vacuole sequestration mechanisms of rutile NPs in *P. sativum* root seemed to work

452 in a more efficient way, even when Ti concentration almost doubled (R800), avoiding

453 interaction of these particles with subcellular components and cell metabolism and moreover

454 limiting the damages already received.

455 The response of the Mix treated samples recalled that of A treated samples not only for root

456 growth inhibition, and oxidative stress but also concerning ultrastructural data. These findings

457 can be explained on the basis of the possible influence of the more toxic anatase inside the

458 Mix treatment.

459 Though biochemical quantitative data of bulk treated roots did not show a correspondence

460 between hydrogen peroxide and TBARS contents, histochemical analysis highlighted a

461 superimposable signal pattern by the two specific probes, suggesting a H_2O_2-dependent

462 membrane damage. The fluorescence signals were distinctive in respect to the other

463 treatments, mainly confined in the root epidermis as well as the outermost and innermost

464 layers of the cortex.

465 A strong H_2O_2 signal in the outer part of root cortex was previously noticed (Ruffini

466 Castiglione et al. 2016) in short-term studies in *V. faba* treated with bulk TiO_2 suspension,

467 indicating this part of the root as a preferential target of the micro-scale TiO_2 particles. Just in

468 that root portion, in our system, nanoparticles and particles of different form and aggregation

469 status were detected by TEM analysis. These nanoparticles could be derived from the biosolid,

470 as already relieved for C2. The cell ultrastructure, characterized mainly by empty cells and

471 often presence of two nuclei, suggested alterations of the division cellular process probably on

472 the phragmoplast formation and microtubules. TiO_2 B material, considered for decades an

473 inert and safe material, conversely confirmed its harmfulness (Ruffini Castiglione et al. 2016),

474   inducing genotoxic effects and extensive cell death, according to its classification as possibly

475   carcinogenic to humans (Group 2B carcinogen, IARC 2010).

476

477   **5. Conclusions**

478

479   These findings allow us to conclude that, in our experimental conditions, the presence of

480   biosolid disturbs plant growth of *P. sativum*, causing cellular damages at root level probably

481   through mechanisms not only oxidative stress-dependent, and involving altered signalling

482   processes. These disturbances may depend on non-humified compounds and/or on the

483   presence of toxic elements and of NPs in the Bs-amended soil, being biosolid one of the

484   major sink of TiO_2 NPs released into the soil environment.

485   The addition of TiO_2 particles in the sludge-amended soil further alters plant growth and

486   elicits oxidative and ultrastructural damages. However, non-typical dose-effect relationship

487   seemed to characterize the plant response in our experimentation, suggesting that the

488   complexity of the Bs-amended soil matrix makes it difficult to foresee particle behaviour and

489   effects on plant. In this context, an integrated approach is particularly useful allowing a

490   complementary structure-function analysis.

491   The most responsiveness treatments were those conducted by the anatase crystal form, alone

492   or mixed with rutile, as well as by the corresponding bulk material, whose inhibiting action

493   was confirmed.

494   Both TiO_2 crystal forms were taken up and compartmentalized by plant cell as a possible

495   defence mechanism, particularly effective for rutile NPs.

496   The results of our work suggest a reflection on the promising use of soil amendments and on

497   the application of nanomaterials and their safety. These practices should be carefully analysed,

498   to establish right regulations over their use, confinement, and disposal for the environmental

499   protection and living organism health.

500

504 **References**

505 Amini S, Maali-Amiri R, Mohammadi R, Kazemi-Shahandasht SS (2017) cDNA-AFLP

506 analysis of transcripts induced in chickpea plants by TiO_2 nanoparticles during cold stress.

507 Plant Physiol Biochem 111: 39-49

508 Bakhshizadeh M, Sazgarnia A, Seifi M, Hadizadeh F, Rajabzadeh G, Mohajeri SA (2017)

509 TiO_2-based mitoxantrone imprinted poly (Methacrylic acid-co-polycaprolctone

510 diacrylate) nanoparticles as a drug delivery system. Curr Pharm Des 23: 2685-2694

511 Barceló AR (2005) Xylem parenchyma cells deliver the H_2O_2 necessary for lignification in

512 differentiating xylem vessels. Planta 220: 747–756

513 Bell IR, Ives JA (2014) Nonlinear effects of nanoparticles biological variability: biological

514 variability from hermetic doses, small particles sizes, and dynamic adaptive interactions.

515 Dose-Response 12: 202–232

516 Bhawana P, Fulekar MH (2012) Nanotechnology: remediation technologies to clean up the

517 environmental pollutants. Res J Chem Sci 2: 90-96

518 Brar SK, Verma M, Tyagi RD, Surampalli RY (2010) Engineered nanoparticles in wastewater

519 and wastewater sludge – Evidence and impacts. Waste Manage 30: 504–520

520 Britto DT, Kronzucker HJ (2002) NH_4^+ toxicity in higher plants: a critical review. J Plant

521 Physiol 159: 567-584

522 Burke DJ, Zhu S, Pablico-Lansigan MP, Hewins CR, Samia ACS (2014) Titanium oxide

523 nanoparticle effects on composition of soil microbial communities and plant

524 performance. Biol Fert Soils 50: 1169–1173

525 Chen C, Tsyusko OV, McNear Jr. DH, Judy J, Lewis RW, Unrine JM (2017) Effects of

526 biosolids from a wastewater treatment plant receiving manufactured nanomaterials on

527 *Medicago truncatula* and associated soil microbial communities at low nanomaterial

528 concentrations. Sci Total Environ 609: 799–806

529   Chuankrerkkul N, Sangsuk S (2008) Current status of nanotechnology consumer products and

530   nano-safety issues. JMMM 18: 75–79

531   Commission Regulation (EU) No 1357/2014 of 18 December 2014 replacing Annex III to

532   Directive 2008/98/EC of the European Parliament and of the Council on waste and

533   repealing   certain   Directives;   https://eur-lex.europa.eu/legal-

534   content/EN/TXT/?uri=CELEX%3A32014R1357, accessed in June 2018

535   Cox A, Venkatachalam P, Sahi S, Sharma N (2016) Silver and titanium dioxide nanoparticle

536   toxicity in plants: A review of current research. Plant Physiol Biochem 107: 147-163

537   Du W, Sun Y, Ji R, Zhu J, Wu J, Guo HJ (2011) TiO_2 and ZnO nanoparticles negatively

538   affect wheat growth and soil enzyme activities in agricultural soil. J Environ Monit 13:

539   822-828

540   El-Sherbiny S, Morsy F, Samir M, Fouad OA (2014) Synthesis, characterization and

541   application of TiO_2 nanopowders as special paper coating pigment. Appl Nanosci 4:

542   305–313

543   Fang J, Shan X, Wen B, Lin J, Owens G (2009) Stability of titania nanoparticles in soil

544   suspensions and transport in saturated homogeneous soil columns. Environ Poll 157:

545   1101-1109

546   Gogos A, Moll J, Klingenfuss F, van der Heijden M, Irin F, Green MJ, Zenobi R, Bucheli TD

547   (2016) Vertical transport and plant uptake of nanoparticles in a soil mesocosm

548   experiment. J Nanobiotech 14: 40

549   Halden RU (2015) Epistemology of contaminants of emerging concern and literature meta-

550   analysis. J Hazard Mat 282: 2-9

551   Hartley-Whitaker J, Ainsworth G, Meharg AA (2001) Copper- and arsenate-induced

552   oxidative stress in *Holcus lanatus* L. clones with differential sensitivity. Plant Cell

553   Environ 24: 713-722

554   EEC   (1986)   http://ec.europa.eu/environment/waste/sludge/index.htm.   Council   Directive

555   86/278/EEC on "The protection of the environment, and in particular of the soil, when

556   sewage sludge is used in agriculture"

557   EPA (1994) https://www.epa.gov/biosolids/biosolids-recycling-beneficial-technology-better-

558   environment. 832-R-94-009 on "Biosolids Recycling: Beneficial Technology for a

559   Better Environment"

560   EPA (1993) https://www.epa.gov/biosolids/biosolids-laws-and-regulations#compliance. On

561   "Wastewater Management".

562   IARC—International Agency for Research on Cancer, 2010. Monographs 93. Titanium

563   Dioxide. http://monographs.iarc.fr/ENG/Monographs/vol93/mono93-7.pdf.

564   Italian Legislative Decree n°99/1992, Implementation of Directive 86/278 / EEC, concerning

565   the protection of the environment, in particular of the soil, in the use of sludge in

566   agriculture, Official Gazette, No. 38, 15 February 1992, Ordinary Supplement No. 28.

567   Jana S, Choudhuri MA (1982) Glycolate metabolism of three submerged aquatic angiosperm

568   during aging. Aquatic Bot 12: 345-354

569   Josko I, Oleszczuk P (2013) The influence of ZnO and TiO_2 nanoparticles on the toxicity of

570   sewage sludges. Environ Sci Processes and Impacts 15: 296-306

571   Karnovsky MJ (1965) A formaldehyde-glutaraldehyde fixative of high osmolality for use in

572   electron microscopy. J Cell Biol 27: 137-138

573   Kim B, Murayama M, Colman BP, Hochella F Jr (2012) Characterization and environmental

574   implications of nano- and larger TiO_2 particles in sewage sludge, and soils amended

575   with sewage sludge. J Environ Monitor 14: 1129-1137

576   Kim HJ, Triplett B (2008) Involvement of extracellular Cu/Zn superoxide dismutase in cotton

577   fiber primary and secondary cell wall biosynthesis. Plant Signal Behav 3: 1119–1121

578

579 Kovácik J, Babula P, Hedbavny J, Švec P (2014) Manganese-induced oxidative stress in two
580   ontogenetic stages of chamomile and amelioration by nitric oxide. Plant Sci 215-216: 1-
581   10

582 Larue C, Laurette J, Herlin-Boime N, Khodja H, Fayard B, Flank AM, Brisset F, Carriere M
583   (2012) Accumulation, translocation and impact of TiO_2 nanoparticles in wheat (*Triticum*
584   *aestivum* spp.): influence of diameter and crystal phase. Sci Total Environ 431: 197–208

585 Laxma Reddy PV, Hernandez-Viezcas J-A, Peralta-Videa JR, Gardea-Torresdey JL (2016)
586   Lessons learned: are engineered nanomaterials toxic to terrestrial plants? Sci Total
587   Environ 568: 470–479

588 Li X, Yang Y, Jia L, Chen H, Wei X (2013) Zinc-induced oxidative damage, antioxidant
589   enzyme response and proline metabolism in roots and leaves of wheat plants.
590   Ecotoxicol Environ Saf 89: 150–157

591 Li X, Yang Y, Zhang J, Jia L, Li O, Zhang T, Qiao K, Ma S (2012) Zinc induced
592   phytotoxicity mechanism involved in root growth of *Triticum aestivum* L. Ecotoxicol
593   Environ Saf 86: 198-203

594 Liang D, White RG, Waterhouse PM (2014) Mobile gene silencing in *Arabidopsis* is
595   regulated by hydrogen peroxide. PeerJ 2:e701; DOI 10.7717/peerj.701

596 Liu WK (2011) TiO_2-NPs application in agriculture: a review. In *Agricultural Research*
597   *Updates* (ed B.P. Hendriks), pp. 137–145. Nova Publisher, Hauppage, New York

598 Lu Q, He ZL, Stoffella PJ (2012) Land application of biosolids in the USA: a review. Applied
599   and Environmental Soil Science 2012 : Article ID 201462
600   http://dx.doi.org/10.1155/2012/201462

601 Lyu S, Wei X, Chen J, Wang C, Wang X, Pan D (2017) Titanium as a beneficial element for
602   crop production. Front Plant Sci 8: 597

603 Maurer-Jones MA, Ian L, Gunsolus IL, Murphy KJ, Haynes CL (2013) Toxicity of
604   engineered nanoparticles in the environment. An Chem 85: 3036–3049

605 Muccifora S (2008) Effects of copper on spore germination, growth and ultrastructure of
606   *Polypodium cambricum* L. gametophytes. Environ Poll 153: 369-375

607 Musetti R, Sanità di Toppi L, Martini M, Ferrini F, Loschi A, Favali MA, Osler R (2005)
608   Hydrogen peroxide localization and antioxidant status in the recovery of apricot plants
609   from European Stone Fruit Yellows. Eur J Plant Pathol 112: 53–61

610 Pachapur VL, Larios AD, Cledón M, Brar SK, Verma M, Surampalli RY (2016) Behaviour
611   and characterization of titanium dioxide and silver nanoparticles in soils. Sci Total
612   Environ 563–564: 933–943

613 Petrov VD, Van Breusegem F (2012) Hydrogen peroxide-a central hub for information flow
614   in plant cells. AoB PLANTS pls014; DOI:10.1093/aobpla/pls014

615 Pittol M, Tomacheski D, Simões DN, Ribeiro VF, Santana CRM (2017) Macroscopic effects
616   of silver nanoparticles and titanium dioxide on edible plant growth. Environ Nanotech
617   Monit Manag 8: 127-133

618 Prakash MG, Chung IM (2016) Determination of zinc oxide nanoparticles toxicity in root
619   growth in wheat (*Triticum aestivum* L.) seedlings. Acta Biol Hung 67: 286–296.

620 Rauret G (1998) Extraction procedures for the determination of heavy metals in contaminated
621   soil and sediment. Talanta 46: 449-455.

622 Remédios C, Rosário F, Bastos V (2012) Environmental nanoparticles interactions with
623   plants: morphological, physiological, and genotoxic aspects. J Botany 2012: Article ID
624   751686, http://dx.doi.org/10.1155/2012/751686

625 Rico CM, Majumdar S, Duarte-Gardea M, Peralta-Videa JR, Gardea-Torresdey JL (2011)
626   Interaction of nanoparticles with edible plants and their possible implications in the food
627   chain. J Agric Food Chem 59: 3485–3498

628　Ruffini Castiglione M, Cremonini R (2009) Nanoparticles and higher plants. Caryologia 62:

629　　　　161–165

630　Ruffini Castiglione M, Giorgetti L, Cremonini R, Bottega S, Spanò C (2014) Impact of TiO_2

631　　　　nanoparticles on *Vicia narbonensis* L.: potential toxicity effects. Protoplasma 251:

632　　　　1471–1479

633　Ruffini Castiglione M, Giorgetti L, Bellani L, Muccifora S, Bottega S, Spanò C (2016) Root

634　　　　responses to different types of TiO_2 nanoparticles and bulk counterpart in plant model

635　　　　system *Vicia faba* L. Environ Exp Bot 130: 11–21

636　Siddiqi KS, Husen A (2017) Plant response to engineered metal oxide nanoparticles.

637　　　　Nanoscale Res Lett 12: 92 DOI 10.1186/s11671-017-1861-y

638　Simonin M, Richaume1 A, Guyonnet JP, Dubost A, Martins JMF, Pommier T (2016)

639　　　　Titanium dioxide nanoparticles strongly impact soil microbial function by affecting

640　　　　archaeal nitrifiers. Sci Reports 6: 33643 | DOI: 10.1038/srep33643

641　Song U, Shin M, Lee G, Roh J, Kim Y, Lee EJ (2013) Functional analysis of TiO_2

642　　　　nanoparticle toxicity in three plant species. Biol Trace Element Res 155: 93–103

643　SSSA book series (1996) In Methods of soil analysis, Part 3 - Chemical Methods (ed D.L.

644　　　　Sparks), Soil Science Society of America Inc., Madison, USA

645　Sun TY, Gottschalk F, Hungerbühler K, Nowack B (2014) Comprehensive probabilistic

646　　　　modelling of environmental emissions of engineered nanomaterials. Envir Poll 185: 69–

647　　　　76

648　Tassi E, Giorgetti L, Morelli E, Peralta-Videa JR, Gardea-Torresdey JL, Barbafieri M. (2017)

649　　　　Physiological and biochemical responses of sunflower (*Helianthus annuus* L.) exposed

650　　　　to nano-CeO_2 and excess boron: Modulation of boron phytotoxicity. Plant Physiol

651　　　　Biochem 110: 50-58

652 Tassi EL, Pini R, Gorini F, Valadao I, De Castro JA (2012) Chemical and physical properties

653   of soil influencing TiO₂ nanoparticles availability in terrestrial ecosystems. J Environ

654   Res Develop 6: 1014-1018

655 Thounaojam TC, Panda P, Mazumdar P, Kumar D, Sharma GD, Sahoo L, Panda S (2012)

656   Excess copper induced oxidative stress and response of antioxidants in rice. Plant

657   Physiol Biochem 53: 33-39

658 Tourinho P, van Gestel CA, Lofts S, Svendsen C, Soares AM, Loureiro S (2012) Metal-based

659   nanoparticles in soil: fate, behavior, and effects on soil invertebrates. Environ Toxic

660   Chem 31: 1679–1692

661 Villatte G, Massard C, Descamps S, Sibaud Y, Forestier C, Awitor KO (2015) Photoactive

662   TiO₂ antibacterial coating on surgical external fixation pins for clinical application. Inter

663   J Nanomed 10: 3367–3375

664 Walz C, Juenger M, Schad M, Kehr J (2002) Evidence for the presence and activity of a

665   complete antioxidant defence system in mature sieve tubes. Plant J 31: 189-197

666 Wang WK, Chen JJ, Zhang X, Huang YX, Li WW, Yu HQ (2016) Self-induced synthesis of

667   phase-junction TiO₂ with a tailored rutile to anatase ratio below phase transition

668   temperature. Sci Rep 6:20491 | DOI: 10.1038/srep20491

669 Weir A, Westerhoff P, Fabricius L, Hristovski K, von Goetz N (2012) Titanium dioxide

670   nanoparticles in food and personal care products. Environ Sci Technol 46: 2242–2250

671 Wen G , Bates TE, Inanaga S, Voroney RP, Hamamura K, Curtin D (2002) A yield control

672   approach to assess phytoavailability of Zn and Cu in irradiated, composted sewage

673   sludges and composted manure in field experiments: II. Copper. Plant Soil 246: 241–248

674 Wendehenne D, Gao QM, Kachroo A, Kachroo P (2014) Free radical-mediated systemic

675   immunity in plants. Curr Opin Plant Biol 20: 127–134

676 Yang Y, Wang Y, Westerhoff P, Hristovski K, Jin VL, Johnson MVV, Arnold JG (2014)

677   Metal and nanoparticle occurrence in biosolid-amended soils. Sci Total Environ 485–

678   486:441–449

679 Zheng L, Hong F, Lu S, Liu C (2005) Effect of nano-TiO$_2$ on strength of naturally aged seeds

680   and growth of spinach. Biol Trace Elem Res 104:83–91

681 Zubillaga MS, Lavado RS (2006) Phytotoxicity of biosolids compost at different degrees of

682   maturity compared to biosolids and animal manures. Compost Sci Util 14: 267–270

683

684

685

Figure Legends

Fig. 1 Concentration of Titanium in the soil available fraction (left side axis) and in the root

tissues (right side axis) of *Pisum sativum* grown for 28 days in farming soil (C1), in C1

amended with biosolid (C2) and in the presence of 80 and 800 mg/Kg of TiO_2 nanoparticles

(anatase (A), rutile (R), mix anatase+rutile 1:1 ratio (Mix)) and bulk material (B). Values are

mean of n=3 replicates with standard deviation; different letters in the same matrix represent

significant differences (p<0.05), according to ANOVA and *post hoc* Tukey test. C1 and C2

were compared by Student's t-test (p<0.05).

Fig. 2 Cross hand sections of *Pisum sativum* roots grown for 28 days in farming soil (C1); in

C1 amended with biosolid (C2) and in the presence of 80 and 800 mg/Kg of TiO_2

nanoparticles (anatase, rutile, mix anatase+rutile 1:1 ratio) and bulk material. The plate

comprehends representative images of toluidine blue stained root section and of *in situ*

detection of H_2O_2 by Amplex UltraRed Reagent.

Fig. 3 Cross hand sections of *Pisum sativum* roots grown for 28 days in farming soil (C1); in

C1 amended with biosolid (C2) and in the presence of 80 and 800 mg/Kg of TiO_2

nanoparticles (anatase, rutile, mix anatase+rutile 1:1 ratio) and bulk material. The plate

comprehends representative images of toluidine blue stained root section and of *in situ*

detection of lipid peroxidation by BODIPY 581/591 C11.

Fig. 4 TEM images of: **a**) aggregates of TiO_2 anatase nanoparticles (NPs); **b**) aggregates of

TiO_2 rutile NPs; **c**) portion of control (C1) root cell: the arrow indicates endoplasmic

reticulum; **d-f)** portion of C1 amended with biosolid (C2) root cells: **e**) the arrows indicate the

711   NPs adherent to cell wall near to central cylinder; **f**) the arrow indicates dense particles

712   aggregates in parenchima cells near to rizoderma. V, vacuole; M, mitochondrion; C,

713   chromathin; CW cell wall.

714

715   **Fig. 5** TEM images of **a**) nanoparticles (NPs) (arrows) in cell vacuole of rutile treated root

716   (R800 sample); **b**) portion of cell vacuole of rutile treated root: not recognisable organelles

717   (O) and vesicles (Ve) in zones surrounded by double membrane; the arrows indicate NPs

718   (R800); **c-e**) portions of anatase treated root cells, the arrowhead indicate a crystal in a

719   mitochondrion (M), the arrows indicate NPs in the cytoplasm (**c**: A800, **d**: A80; **e**: A80); **f**)

720   NPs (arrows) in vacuoles and in vesicles (Ve) in anatase treated cell root (A80). N, nucleus;

721   V, vacuole.

722

723   **Fig. 6** TEM images of **a, b**) portion of cells near to rizoderma of anatase treated roots, the

724   arrows indicate Nanoparticles (NPs) in a mitochondrion (M) and in the cytoplasm (**a**: A800;

725   **b**: A80); **c**, **d**) anatase NPs (arrows) adherent, crossing cell wall (CW) and in the intercellular

726   space (IS) (A800); **e**) portion of bulk treated root, the arrows indicate nuclei (B800); **f**) dense

727   large particles aggregate (arrow) in bulk treated cells (B800). CW, cell wall.

728

729

730

731

732

733

734

735

Table 1. Root growth and oxidative stress (hydrogen peroxide and thiobarbituric acid reactive substances, TBARS) in *Pisum sativum* plants grown for 28 days in farming soil (C1); in C1 amended with biosolid (C2) (**a**) and in the presence of 80 and 800 mg/Kg of TiO$_2$ nanoparticles (anatase, A; rutile, R; mix anatase+rutile 1:1 ratio) and bulk material, B (**b**). Data are reported as mean values ± SE. Means followed by the same letters within the same row are not significantly different at 5%.

a)

	C1	C2
Root Length (cm)	12.92±0.80a	10.69±0.33b
Hydrogen peroxide (µmol/gFW)	1.07±0.06a	0.97±0.07a
Lipid peroxidation (nanomol/gFW)	28.54±0.35a	28.87±0.86a

b)

	C2	R80	A80	Mix80	B80	R800	A800	Mix800	B800
Root Length (cm)	10.69±0.33a	8.82±0.57b	7.00±0.38c	8.10±0.42bc	7.71±0.58bc	8.60±0.52b	9.11±0.44b	9.18±0.55b	7.17±0.57c
Hydrogen peroxide (µmol/gFW)	0.97±0.07de	0.76±0.05ef	2.05±0.08a	1.47±0.08b	1.15±0.11cd	1.26±0.08bc	0.95±0.17def	0.68±0.08f	1.28±0.13bc
TBARS (nanomol/gFW)	28.87±0.86b	26.81±0.50cd	28.83±0.34b	28.68±0.20bc	26.14±0.13d	25.28±0.22d	25.93±0.46d	31.82±0.70a	26.14±0.19d

737

738

739

740

741

742

743

744

745

746

747

748
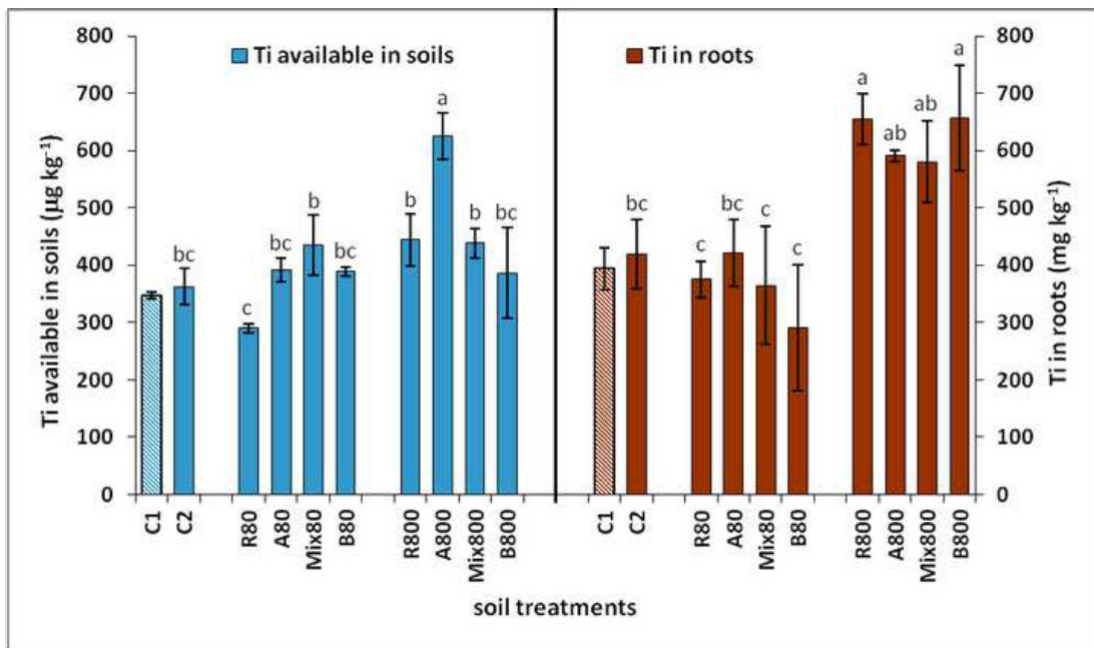
749

750

751

752

753

754   Figure 1
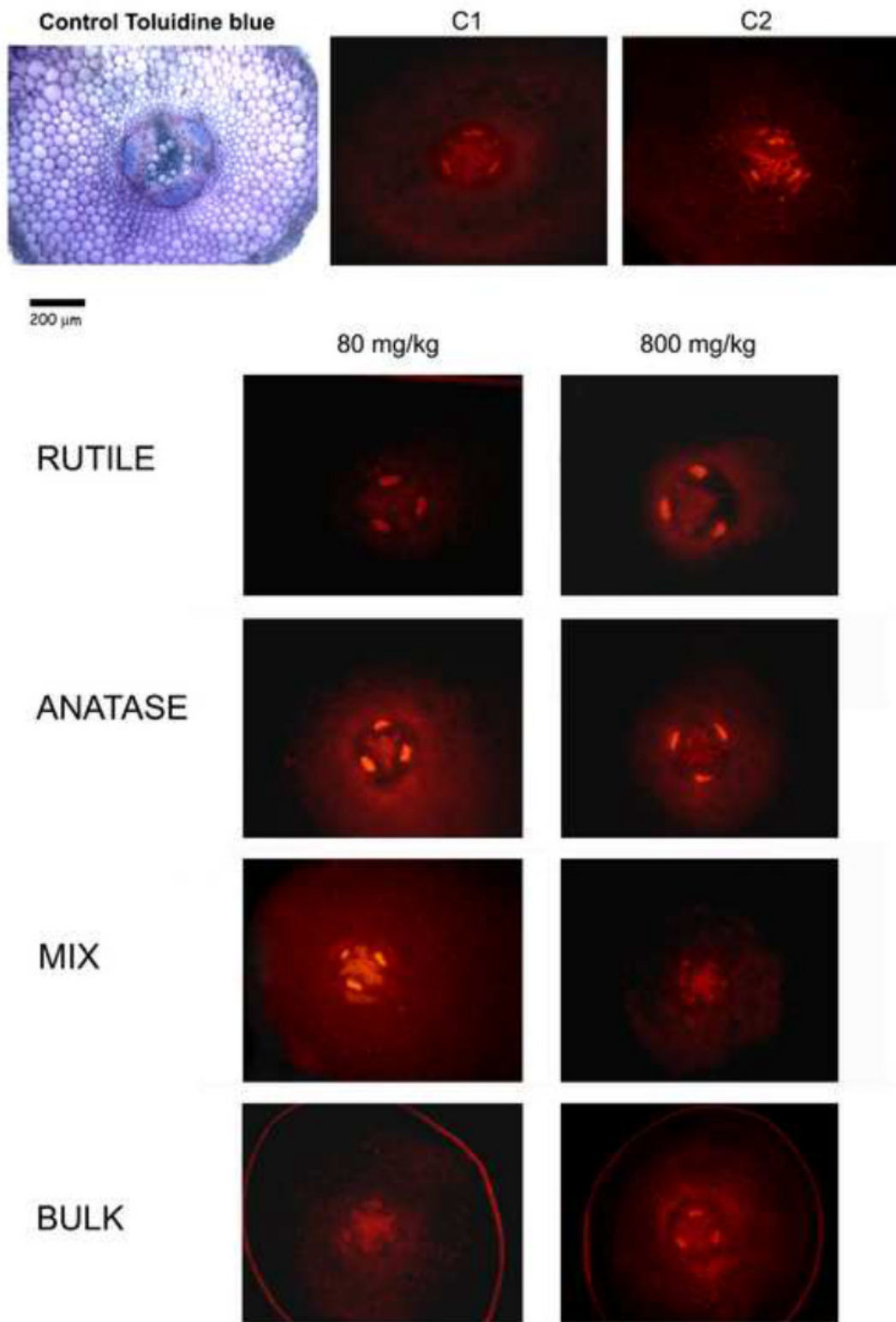
755

756

757

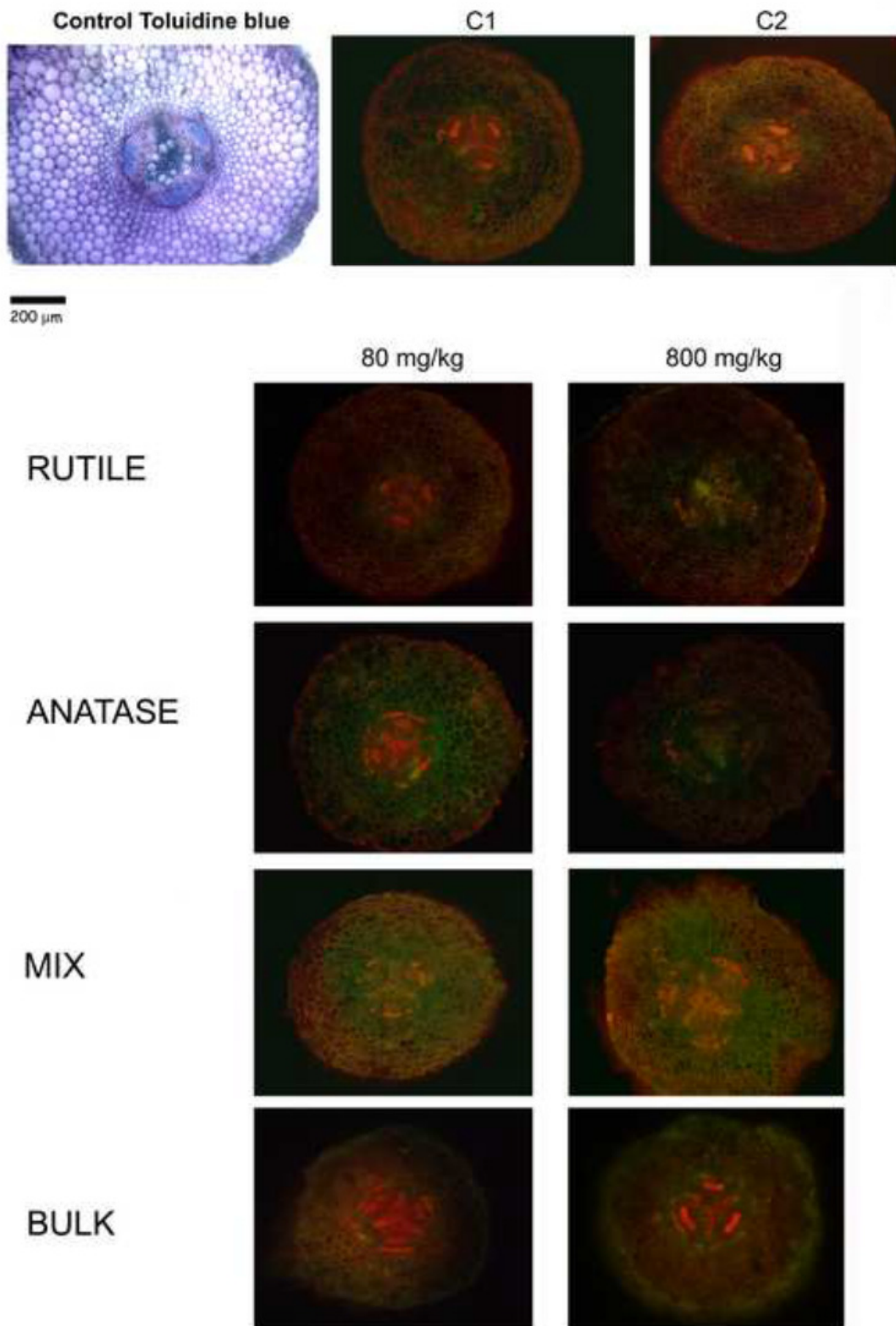758

759

760

761

762

763

764

765

766

767

768

769

770   Figure 2

773   Figure 3

Control Toluidine blue   C1   C2

200 µm

80 mg/kg   800 mg/kg

RUTILE

ANATASE

MIX

BULK

774

775

776   Figure 4

779   Figure 5